

# Exploratory seismic site response surveys in a complex geologic area: a case study from Mt. Etna volcano (southern Italy)

F. Panzera<sup>1</sup> · G. Lombardo<sup>1</sup> · E. Longo<sup>3</sup> · H. Langer<sup>2</sup> ·  
S. Branca<sup>2</sup> · R. Azzaro<sup>2</sup> · V. Cicala<sup>1</sup> · F. Trimarchi<sup>1</sup>

Received: 16 December 2015 / Accepted: 3 August 2016 / Published online: 6 August 2016  
© Springer Science+Business Media Dordrecht 2016

**Abstract** A preliminary study targeting to evaluate the local seismic response was performed in the eastern flank of Mt. Etna (southern Italy) using ambient noise measurements. The obtained spectral ratios were subdivided through cluster analysis into different classes of fundamental frequency permitting to draw an iso-frequency contour map. The analysis set into evidence the extreme heterogeneity of lava sequences, which makes difficult to identify a single seismic bedrock formation. Another important outcome, concerning the local seismic effects in terms of frequency and azimuth, is the important role played by the fracture fields associated with the main structural systems of the area. The existence of two zones with strong directional effects striking WNW–ESE and NW–SE, nearly orthogonal to the orientation of the main fracture fields, corroborate such hypothesis.

**Keywords** Spectral ratios · Seismic site response · Seismic wave polarization · Directional effect · Cluster analysis

## 1 Introduction

Microzoning an area for earthquake ground motion purposes is one of the fundamental aspects of seismic risk assessment. Seismic input acting on buildings is related to surface ground motion features that depend on location and magnitude of the earthquakes, seismic attenuation, and local site effects. These parameters are tightly linked to the characteristics of the investigated area in terms of the presence of soft soils, hill slopes, and structural

---

✉ F. Panzera  
panzerafrancesco@hotmail.it

<sup>1</sup> Dipartimento di Scienze Biologiche, Geologiche e Ambientali, Università degli Studi di Catania, Catania, Italy

<sup>2</sup> Osservatorio Etno, Istituto Nazionale di Geofisica e Vulcanologia, Catania, Italy

<sup>3</sup> Department of Geosciences, University of Malta, Msida, Malta

discontinuities (faults and fractures). Then, site effects should be considered a crucial issue in researches aiming to assess the earthquake ground motion. Generally, a study for seismic site classification is based on data coming from boreholes, geologic surveys, and geophysical prospecting. Most of the international seismic codes make use of the average shear wave velocity of the upper 30 m ( $V_{S,30}$ ) to discriminate soil categories (e.g., Eurocode8 2003). Some doubts, however, arise whether  $V_{S,30}$  is a suitable parameter for estimating the actual soil amplification especially in complex geologic zones such as volcanic areas. As shown in recent studies, on Mt. Etna we deal with the presence of frequent and marked lateral heterogeneities, due to lavas and sediments that exhibit complex stratigraphic relationships with strong lateral and vertical variations (Panzera et al. 2011a). The picture is further complicated by fractures and tectonic discontinuities linked to the architecture of the fault zone (Panzera et al. 2014, 2016) and the occurrence of significant vertical velocity inversions (Panzera et al. 2015). In spite of these complications, information on seismic site response can be achieved by using microtremor measurements. In particular, a quick estimate of the site effects role in the seismic motion observed at the surface can be provided by the horizontal to vertical noise spectral ratio technique (HVNR). This method, introduced by Nogoshi and Igarashi (1971), was reformulated by Nakamura (1989) and became in recent years widely used. Many authors (e.g., Mucciarelli 1998; Rodriguez and Midorikawa 2002; Maresca et al. 2003) have questioned the existence of simple direct correlation between HVNR amplitude values and site amplification, since the ambient noise appears actually made of an unpredictable brew of different wavefields, rather than Rayleigh waves alone. Nonetheless, as demonstrated by Lermo and Chavez-Garcia (1993), it provides a reliable estimate of the fundamental frequency of soil deposits.

In the Etna area, the role of site effects in amplifying seismic ground motion has been recognized for Catania, the principal city (ca. 500,000 inhabitants) of Eastern Sicily that is exposed to relevant seismic risk due to regional earthquakes (Azzaro et al. 1999, 2008). Here, several studies focused on investigating the role of the stratigraphy or morphology in inducing resonance phenomena at the urban scale, were performed (Langer et al. 1999; Romanelli and Vaccari 1999; Panzera et al. 2011a, 2015). The main goal of this work is extending to the whole eastern flank of the volcano a first identification of sites potentially prone to ground motion amplification following a seismic input. This area is particularly interesting since it is characterized by high spatial variability of the geologic features, which are also largely hidden by urbanization. Moreover, from the seismotectonic point of view, it is the most active zone of Etna with faults capable of generating shallow earthquakes that produce destructive effects at local scale (Azzaro 2004; Azzaro et al. 2013b; Panzera et al. 2011b). In the study area, both masonry (MA) and reinforced concrete (RC) buildings are widely common. The MA buildings typology was predominant until 1950, whereas the RC buildings reached the maximum development in the 1970s and 1980s and represent the most widespread architectural typologies. It must be noticed that the seismic code provisions were enforced only as late as the 1980s, and this fact, similarly to the main towns in eastern Sicily and southern Italy, has to be taken into account in typecasting the dynamical properties of buildings and the evaluation of their vulnerability. Finally, the densely urbanized setting of the volcano's eastern flank—hosting 27 municipalities over an area of ca. 500 km<sup>2</sup>—as well as the vulnerability of its residential building stock expose towns and villages in the area to a relevant level of seismic risk, even just considering the economic losses determined by direct repair costs (D'Amico et al. 2016).

## 2 Seismotectonic and geologic setting

Mt. Etna is a 3300-m-high basaltic stratovolcano located along the eastern coast of Sicily (Fig. 1b), at the boundary between African and European plates (Polonia et al. 2016). The volcanic edifice shows a diameter of about 40 km and lies at the front of the Sicilian thrust belt and at the footwall of the northern sector of the Malta escarpment delimiting the margin of the Ionian Sea (Finetti et al. 2005; Lentini et al. 2006). Its tectonic setting and present geodynamics result from the interaction of regional tectonics and local-scale volcano-related processes, such as flank instability and dyke-induced rifting (Azzaro et al. 2013a; Gross et al. 2016).

The eastern and southeastern flanks of the volcano are the most tectonically active, being affected by a 20-km-long system of extensional faults (Timpe, TFS in Fig. 1a) characterized by individual escarpments up to 200 m high, that offset late Pleistocene to historical age lava flows with normal-oblique kinematics (Azzaro et al. 2013a). The unstable, E–ESE seaward sliding sector (Bonforte et al. 2011) is delimited to the North by the Pernicana fault system (PFS in Fig. 1a), a 20-km-long left-lateral strike-slip structure featuring the most striking evidence of active tectonics (Neri et al. 2004), with slip-rate higher than 2 cm/yr in the last 200 years (Azzaro et al. 2012 and reference therein). The southern boundary of the sliding flank (SFS in Fig. 1a) is composed of the NW–SE-trending Tremestieri (TMF) and the Trecastagni (TCF) faults, whose dextral-oblique displacement is also accommodated by buried tectonic features revealed through geochemical surveys (Bonforte et al. 2013) and remote sensing data (Neri et al. 2009; Bonforte et al. 2011). The intense tectonic activity of these faults in the eastern sector of Etna, the most urbanized of the volcano, is demonstrated by the recurrence of very strong historical earthquakes determining a high level of seismic hazard (Azzaro et al. 2016). In this area, macroseismic intensities, up to degrees VIII–IX on the European Macroseismic Scale (EMS, see Grünthal 1998), as well as intense creep phenomena (Azzaro et al. 2012), are expected. In particular, the occurrence of extensive coseismic and aseismic surface faulting (Azzaro 2004) produces permanent effects along strike such as fractures, scarplets, and local subsidence, affecting both the superficial layers and the hanging wall bedrock. These ground breakages not only determine damage to man-made features located astride dislocation lines (Azzaro et al. 2010), but may also influence the site response following a seismic input (Panzera et al. 2014).

As regards the lithologic sequence, this region is formed by a complex volcanic succession (for details see Branca et al. 2011a) consisting of overlapping lava flows, whose structure ranges from massive to scoriaceous lavas and subordinately tephra products. Tephra are mainly formed by unwelded fall pyroclastic deposits, rarely lithified, made up of scoriaceous lapilli and ash from fine to coarse, and by lithified pyroclastic flow deposits. Subsurface data evidenced that within the volcanic succession, there are also limited epiclastic deposits and numerous debris and alluvial deposits interlayered along the lower flanks (Branca 2003; Branca and Ferrara 2001). In the investigated area (Fig. 1) the volcanic successions formed during the geological evolution of the past 220 ka through an almost continuous effusive activity of the Timpe phase (Supersynthem of Branca et al. 2011b). For about 110 ka, the central type effusive and explosive activity followed, producing the growth of the composite stratovolcano edifice (Valle del Bove and Stratovolcano phases of Branca et al. 2011b; see Fig. 1). In particular, the Timpe phase consists of a lava flows succession locally interlayered with thick debris and alluvial deposits cropping out along the Acireale and Moscarello fault scarps. The volcanic products erupted during

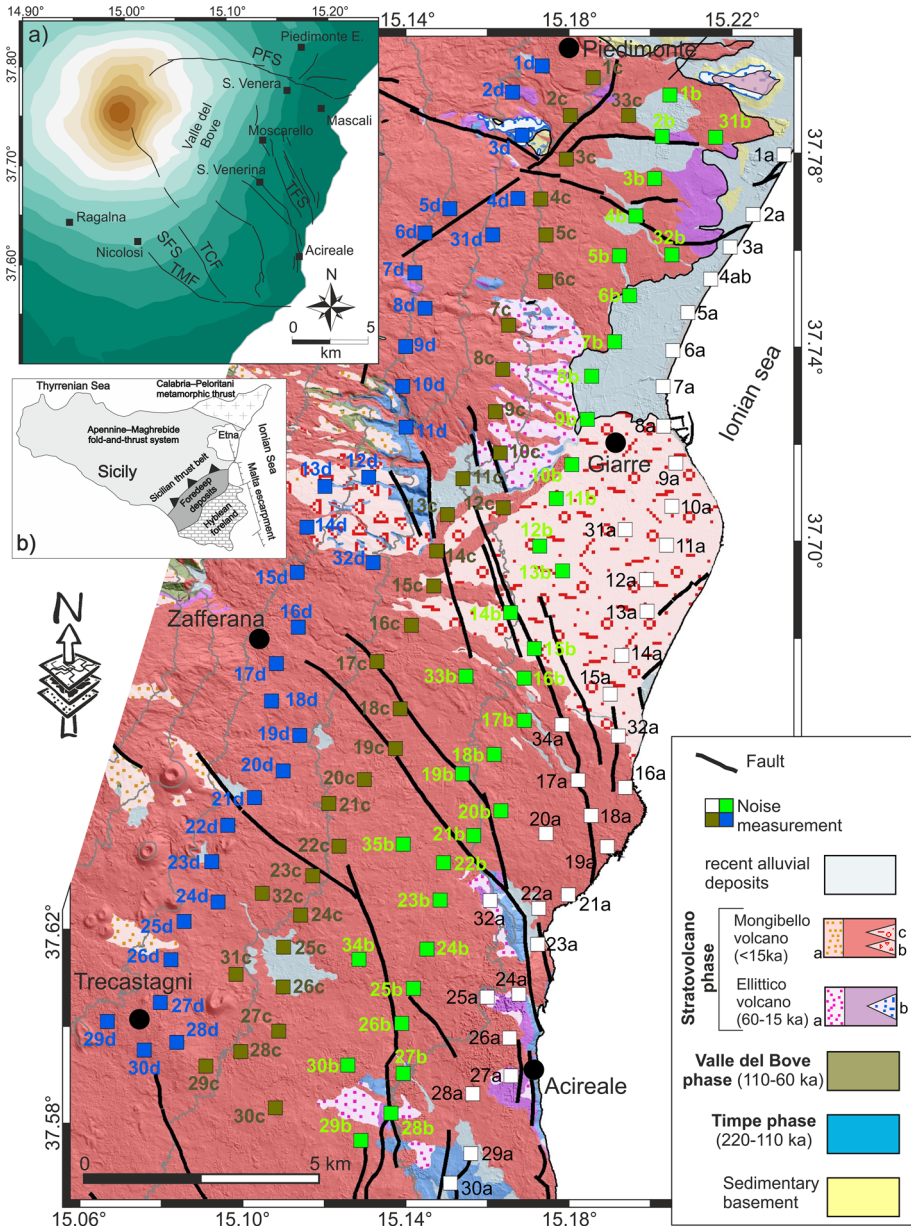


**Fig. 1** Geological map of the investigated area (modified from Branca et al. 2011b). In the Stratovolcano phase, successions of the Ellittico volcano consist of: **a** pyroclastic deposits; **b** debris-alluvial deposits; successions of the Mongibello volcano consist of: **a** pyroclastic deposits; **b** Milo debris deposit; **c** Chiancone alluvial deposit. The inset map (a) shows the main structural features of Mt. Etna eastern flank (modified from Barreca et al. 2013); from north to south: PFS (Pernicana fault system), TFS (Timpe fault system), SFS (Southern fault system), TMF (Tremestieri-Mascalucia fault), and TCF (Trecastagni fault). The inset (b) illustrates the tectonic framework of the study area with major structural domains (modified from Lavecchia et al. 2007)

the last 60 ka formed the main portion of the investigated area. They are represented by the lava and pyroclastic successions of the Ellittico volcano (60–15 ka) and by the volcanics erupted during the last 15 ka related to the Mongibello volcano (Branca et al. 2011a, b). In particular, the intense effusive and explosive activity of Mongibello volcano produced a thick lava succession with interlayer pyroclastic deposits that cover about the 88 % of the Etna's surface (Branca et al. 2011a). In addition to this typology of volcanic rocks, a thick Holocene volcanoclastic succession related to the formation of the Valle del Bove depression crops out immediately eastward of the valley down to the coast (Fig. 1). This succession is formed by a debris avalanche deposit and by a wide fan-shaped detritic–alluvial deposit named “Chiancone” (Branca et al. 2011a, b).

The complex geological evolution of Etna volcano created an extremely heterogeneous volcanic succession, that along the lower eastern flank of Etna exhibits large thickness ranging from 0 up to 900 m (see for details Branca and Ferrara 2013). In particular, the variation of the volcanic pile thickness is highly conditioned by the morphologic setting of the basement underlying Etna. In particular, the eastern flank is characterized by the presence of a deep depression filled by a thick volcanic and volcanoclastic successions characterized by a high lateral and vertical variation of the lithologies (Branca and Ferrara 2013). This basement depression is delimited both to the north and southward by an E–W-elongated morphostructural high of the basement (Vena and Aci Trezza ridge of Branca and Ferrara 2013), where the volcanic pile is <200 m thick. Conversely, along the central portion of the lower eastern flank the volcanic and volcanoclastic successions reached thickness ranging from 600 up to 900 m. Finally, in this sector of Etna the sedimentary basement crops out only in restricted portions of the morphostructural highs, where the Early-Middle Pleistocene marly clays are exposed up to an elevation of 770 m along the Vena Ridge (Branca and Ferrara 2013).

### 3 Methodology

#### 3.1 HVNR and cluster analysis

To investigate about the local seismic response, several strategies could be adopted. A straightforward and not time-consuming approach consists in performing a large number of ambient vibration measurements that highlight areas having homogeneous site response features. To this end, in the lower eastern flank of Etna volcano a grid (spaced  $1.0 \times 1.0$  km) was planned, locating the recording sites at the nodes of it. Since the present study aims at an exploratory site response estimate, we intentionally did not focus the spatial distribution of recording sites with respect to location of the main faults and/or features of the outcropping lithotypes, but we rather preferred a quite regular spacing of measurement points. The ambient noise was recorded in 135 sites (Fig. 1) using Tromino<sup>TM</sup>, a compact three-component velocimeter. This kind of seismometer was preferred to other commercial data logger for its compact configuration that permits a fast installation and then the acquisition of a great amount of data in short time. Using a short period instrument, despite the thickness of the volcanic succession reaches values up to 900 m, could imply the presence of low-frequency effects (<0.5 Hz). On the other hand, the reduced reliability of Tromino<sup>TM</sup> response, at relatively low frequencies, appears not of primary interest for engineering purposes. Studies concerning the dynamic properties of the buildings in eastern Sicily (Panzera et al. 2013 and Panzera et al. 2016)

pointed out indeed that their fundamental periods are lower than 1.0 s ( $>1.0$  Hz). Time series 30 min long were recorded with a sampling rate of 128 Hz (equivalent to 128 samples per second). Following the SESAME (2004) guidelines, the recorded signal was afterward divided in time windows of 30 s not overlapping. For each window, a 5 % cosine taper was applied, and the Fourier spectra were calculated in the frequency range 0.5–20.0 Hz. The spectra of each window were smoothed using a Konno–Ohmachi window (Konno and Ohmachi 1998). In this step it is crucial to set the parameter  $b$  properly. A small value of  $b$  will lead to a strong smoothing, whereas a large value of  $b$  will lead to a low smoothing of the Fourier spectra. Generally, for site response analysis the  $b$  value is fixed equal to 40 (SESAME 2004). Finally the resulting HVNR was computed estimating the logarithmic average of the spectral ratio obtained for each time window, selecting only the most stationary part of the signal and excluding transients associated to very close sources.

The obtained HVNRs were subdivided into groups showing a similar shape using a  $k$ -means cluster analysis (Fig. 2). Such approach has been used in several studies (e.g., Rodriguez and Midorikawa 2002; Cara et al. 2008) aiming to summarize the information coming from the HVNR in order to identify homogeneous areas in terms of site response and local geology. In particular, Cara et al. (2008) clustered sites by considering only the similarities in the HVNR function, whereas Rodriguez and Midorikawa (2002) tested the reliability of the cluster results through the comparison with earthquake spectral ratios. The clustering technique includes different algorithms and methods for grouping objects in a set of categories with relatively homogeneous characteristics. In the present study, the cluster analysis was computed taking into account only the HVNR amplitudes in the 0.5–10.0 Hz frequency range. Higher frequency values ( $>10$  Hz) were not included, being not interesting from the engineering point of view. The analysis was performed taking into account the 135 HVNRs ( $i = 1 \dots 135$ ) whose amplitude was computed at 82 frequency values ( $M$ ) in the range 0.5–10.0 Hz, expressing them by a vector  $y_{iM}$ . The degree of similarity between the HVNRs observed at two sites (e.g.,  $i$  and  $j$ ) was calculated using the Euclidean distance:

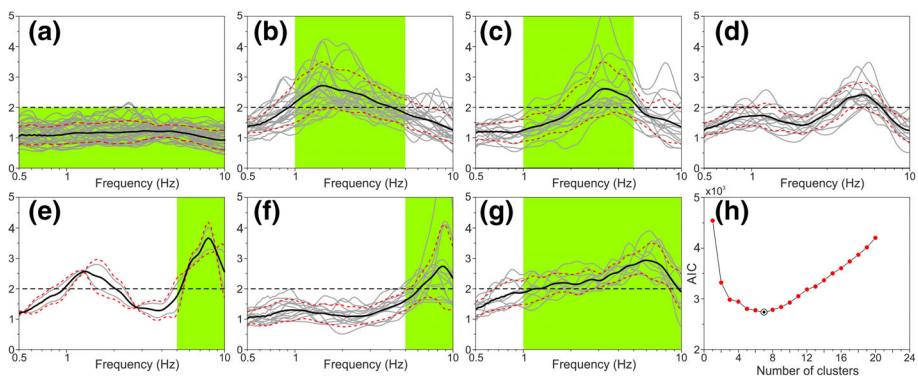


**Fig. 2** HVNR clusters resulting for the Etnean area (a–g). Gray lines refer to each HVNR forming the cluster; black lines show the average HVNR for each cluster; red dashed lines correspond to  $\pm\sigma$  standard deviations; dashed line indicate the significance value of spectral peaks; green area delimitate the frequency range of the observed HVNR peaks. **h** Akaike information criterion parameter versus the number of clusters for the studied area

$$d_{ij} = \sqrt{\sum_{M=1}^{82} (y_{iM} - y_{jM})^2} \tag{1}$$

Finally, the use of *k-means* clustering approach (MacQueen 1967) led to the definition of the clusters. This technique consists in ranking into  $N_C$  clusters, chosen by the user, the  $N_K$  measurement points and evaluating the quality of the clustering by computing the sum of the squared error (SSE):

$$SSE = \sum_{i=1}^{N_K} \sum_{j=1}^M (y_{ij} - y_{C_{kj}})^2 \tag{2}$$

where  $y_{Ck}$  is the centroid of the vectors  $y_i$  in the cluster, calculated through:

$$y_{C_{kj}} = \frac{1}{N_K} \sum_{i=1}^{N_K} y_i \tag{3}$$

The *k-means* algorithm directly attempts to minimize the SSE, assessing each measurement point to its nearest cluster and repeating the computation until the results do not change anymore.

The detection of the optimal number of clusters in a dataset is a general problem (Burnham and Anderson 2002) that can be solved through several methods. In the present paper the identification of the best solution from a group of acceptable models was achieved through the Akaike information criterion (AIC, Akaike 1974). This procedure does not require particular assumptions on the experimental data and is suitable for solving the model decision problem in many applications (Burnham and Anderson 2002). To find the optimal number of clusters, the analysis was run for increasing values of NC (ranging from 1 to 20) and selecting the NC value for which the AIC is minimized. Assuming that the model error is normally distributed, the AIC formula is:

$$AIC = N_K \ln\left(\frac{RSS}{N_K}\right) + 2k + \frac{2k(k + 1)}{(N - k - 1)} \tag{4}$$

where  $N_K$  is the total number of HVNR,  $\ln$  indicates the natural logarithm, RSS is the residual sums of squares and  $k$  indicates the number of free parameters as  $N_C - 1$ . In the present study RSS is defined as the sum of the SSE of all the clusters.

### 3.2 Investigations on directional effects

The experimental spectral ratios were also calculated after rotating the horizontal components of motion by steps of 10 degrees starting from 0° (north) to 180° (south), using the same criteria (windows length, taper, smoothing) adopted for HVNR. This analysis was performed in order to investigate about the possible presence of directional effects. Examples of the results obtained are plotted in Fig. 3 using contour plots of amplitude, as a function of frequency (x-axis) and direction of motion (y-axis). We also performed a direct estimate of the polarization angle by using the covariance matrix method (Jurkevics 1988) to overcome the bias linked to the denominator behavior that could occur in the HVNR technique. This technique is based on the evaluation of eigenvectors ( $u_1; u_2; u_3$ ) and eigenvalues ( $\lambda_1; \lambda_2; \lambda_3$ ) of the covariance matrix obtained by three-component

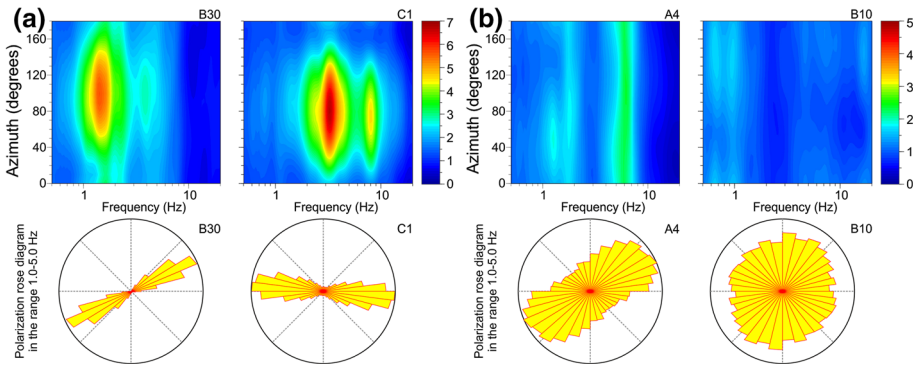


**Fig. 3** Examples of contours of the spectral ratios geometric mean, as a function of HVNR amplitudes (color scale), frequency (x-axis) and direction of motion (y-axis), with corresponding polarization rose diagrams. **a** Shows the results obtained at sites with strong directional effects, **b** displays examples of results obtained at sites with no evidence of directional effects

seismograms. Parameters describing the characteristics of the particle motion (rectilinearity  $L$ ; azimuth  $A$ ; incidence angle  $I$ ) are extracted using the attributes from the principal axes. In particular, the degree of rectilinearity is defined as:

$$L = 1 - \left( \frac{\lambda_2 + \lambda_3}{2\lambda_1} \right) \tag{5}$$

and it is equal to unity for pure body waves and zero for spherical waves. The azimuth of a wave can be estimated by:

$$A = \tan^{-1} \left( \frac{u_{21}(\text{sign } u_{11})}{u_{31}(\text{sign } u_{11})} \right) \tag{6}$$

where  $u_{1j}$   $j = 1, 2, 3$  are the three direction cosines of the eigenvector  $u_1$  and the *sign* function is introduced to resolve the ambiguity of taking the positive vertical component of  $u_1$ . The apparent incidence angle of rectilinear motion may be obtained from the corresponding direction cosine of  $u_1$ :

$$I = \cos^{-1} |u_{11}| \tag{7}$$

Signals at each site were band-pass-filtered using the entire recordings and a moving window of 1 s with 20 % overlap, therefore obtaining the strike of maximum polarization for each moving time window. To summarize the general trend of the polarization azimuth at each site, rose diagrams were depicted (Fig. 3). Each diagram displays a circular histogram in which instantaneous polarization azimuth measurements are plotted as sectors of circles with a common origin (bin size 10°).

### 4 Results and discussion

The HVNRs obtained from measurements performed in the eastern flank of Etna volcano were subdivided into 7 clusters (see results in Fig. 2) according to the minimum value reached by the AIC (see panel (h) in Fig. 2).



The cluster (a) consists of 39 measurements characterized by flat HVNR (amplitude lower than 2 units) in the frequency range 0.5–10.0 Hz. The HVNRs in the clusters (b) and (c) are altogether 43, and show dominant peaks at about 1.5 and 3.0 Hz, respectively. The cluster (d) is composed by 13 spectral ratios with dominant frequency at about 5.0 Hz. High-frequency HVNR peaks (>5.0 Hz) are observed in 15 sites that were included in the clusters (e) and (f). Finally, the cluster (g) is characterized by nine spectral ratio curves broadly trending toward an increase in amplitude. The above-described clusters were further merged in four classes taking into account the shape similarities (see green shadowed areas in Fig. 2). In particular, the identified classes are: (I) flat HVNR, cluster (a), (II) broadband behavior, cluster (g), (III) spectral ratios with fundamental frequency in the range 1.0–5.0 Hz, clusters (b) and (c), and (IV) high-frequency peaks (>5.0 Hz), cluster (e) and (f). The cluster (d), having a bimodal shape with spectral ratios that can be partially ascribed to both classes III and IV, was removed and the related HVNRs were accordingly subdivided. Finally, the HVNRs included in each group were checked to verify the reliability of the obtained classification. The check confirmed the consistency of the adopted cluster analysis showing that almost 90 % of HVNRs belong to each assigned group, and the remaining 10 % was manually re-allocated. The large number of measurements available, with a quite homogeneous spacing, allowed us to draw a macro-zones contour map of the studied area, discriminating sites having different “fundamental frequency classes” (Fig. 4). It was attained through the nearest neighborhood algorithm subdividing the study area into cells, using the Voronoi diagram method, and defining for each point its influence area through a Delaunay triangulation. Inspection of the map (Fig. 4) points out that it is very difficult to interpret the results in term of the outcropping lithologies. A rather good matching is observed only for the Chiancone area (to the south of the town of Giarre, see location in Fig. 1) where flat spectral ratios were usually observed. This finding is consistent with the nature of the volcanoclastic conglomerate deposit, which is poorly stratified and often hardened. The overall thickness of this unit inferred by borehole data and geophysics investigations is about 300 m (Branca et al. 2011a). It is also worth noting that the map shows wide areas, delimitating both the fundamental frequencies in the ranges  $1.0 \leq F_0 < 5.0$  Hz and some broadband spots (see blue and red areas in Fig. 4). Although in these zones lava formations outcrop extensively, the presence of such amplification effects clearly points out the presence of several local discontinuities that delineate alternating soft and stiff layers. Moreover, inspection of Fig. 4 sets also into evidence that these areas stretch out in a direction consistent with that of the main faults. This behavior is clearly evident in the southern part of the study area (Zafferana, Acireale, Trecastagni) and around the TFS, whereas it is only partially evident to the north of the PFS. The above considerations are confirmed by 2-D diagrams (Fig. 5) obtained by combining all the ambient noise measurements performed along each transects (see different color measurement sites located in Fig. 1). These profiles highlight that it is quite hard to identify a continuous bedrock formation, whereas heterogeneities producing resonance effects are detected. It is also evident that transects (a) and (b) in Fig. 5 show in their SW part—where the TFS has a major geomorphic expression—that amplification site effects are particularly marked. In the (c) and (d) transects such effects spread all over the 2-D diagrams. This could be related to the existence of a more diffused fractured area linked to the fault zone.

Most of the investigated sites show a significant amplitude increment of rotated HVNRs in the frequency range 1.0–5.0 Hz (see examples in Fig. 3). These results highlight a preferential and site-dependent direction of the horizontal ground motion amplification. The investigated area is indeed extremely heterogeneous from the lithologic and structural point of view. More in detail, the existence of different fault systems (the WNW–ESE-

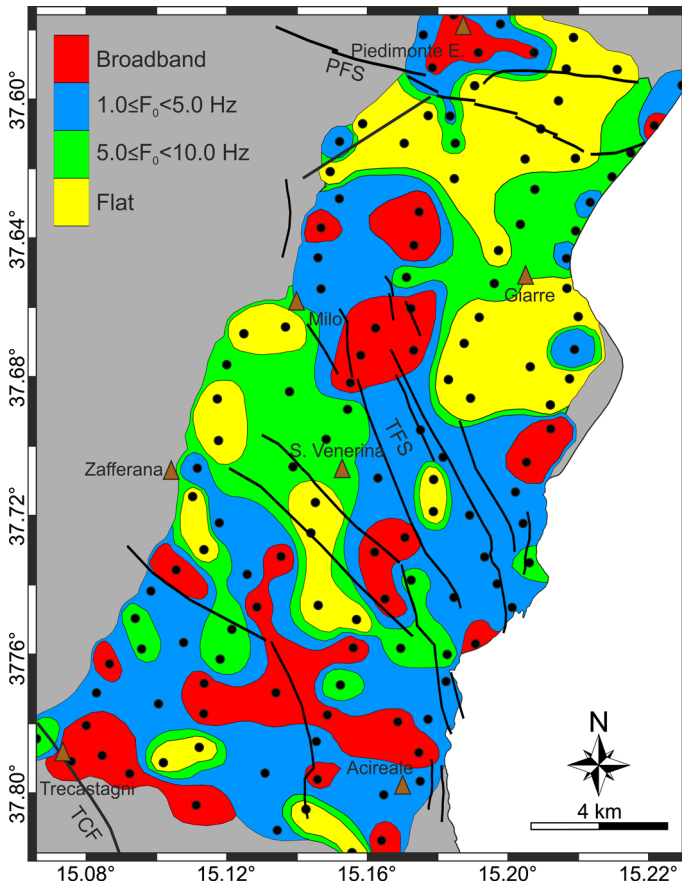


**Fig. 4** Contour map bounding sites having different spectral ratio features

striking PFS and the NW–SE-striking TFS and SFS) can induce a preferential polarization direction of seismic waves as observed and described in other studies investigating the wavefield polarization along faults at Etna (Rigano et al. 2008; Di Giulio et al. 2009; Pischitta et al. 2013; Panzera et al. 2014; Imposa et al. 2015; Panzera et al. 2016). To confirm the HVNR results and support our hypothesis that the directional effects are linked to a heterogeneous medium characterized by oriented fractures, a polarization analysis was performed. It is interesting to observe that azimuth polar plots clearly show a pronounced polarization in the frequency band 1.0–5.0 Hz, with maxima trending almost perpendicularly with respect to the faults (Fig. 6). In particular, three different zones are identified. The first, to the North, encloses PFS (see inset in Fig. 1a), in which rose diagrams show a prevalent NE–SW direction. The second zone is characterized by scattered or low polarization and the third one including TFS and TCF, represents the largest area with almost E–W-trending polarization. It should be stressed that this area includes the sector investigated in the frame of a project funded by the Sicilian Civil Protection (Azzaro et al. 2010) aimed at mapping fractures and cracks that may induce or enhance damage to buildings during earthquakes. The study identified 26 fracture zones between Acireale, Santa Venerina e Milo that were mostly oriented N–S in the area of Acireale, and NNW–SSE in the areas of

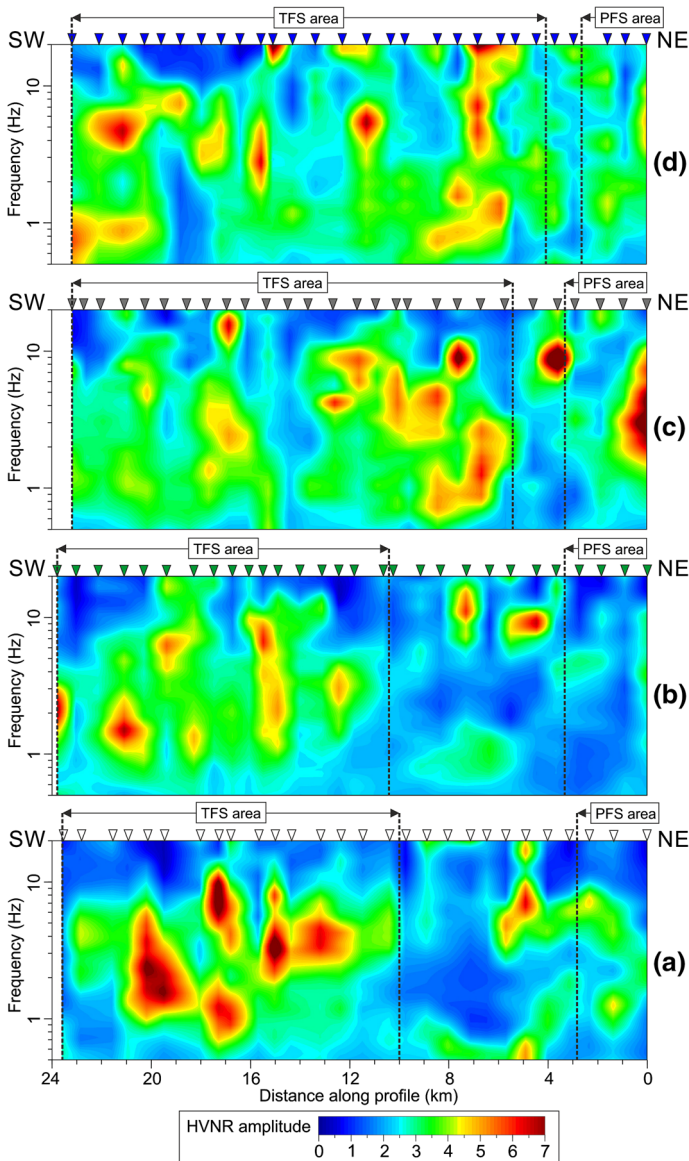


**Fig. 5** 2-D diagrams obtained by combining all the ambient noise records performed along the transects **a–d** (see Fig. 1) as a function of distance (*x*-axis), frequency (*y*-axis) and HVNR contour plot amplitudes

Santa Venerina and Milo. Taking into account the results of this structural survey and the aforementioned studies concerning features of the seismic site response along fault zones in the Etna area, the observed wavefield polarization could be interpreted as linked to the presence of these secondary cracks and fractures. The prevalence of a specific polarization azimuth, especially in the zones I and III (Fig. 6), is therefore determined by the strong anisotropic effects linked to the oriented fractures existing in the damage fault area (e.g., Pischiutta et al. 2014). In such conditions, different attenuation properties of the body

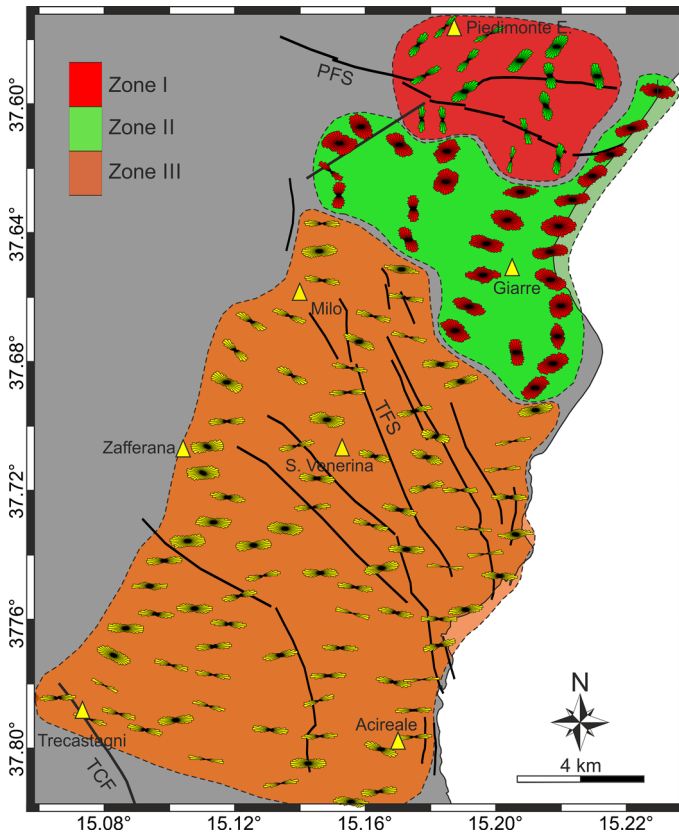


**Fig. 6** Rose diagrams of the polarization azimuth in the frequency range 1.0–5.0 Hz for each measurement site. The different colored areas gather together rose diagrams showing similar features and/or prevailing azimuths

waves take place, and in particular P waves appear more attenuated perpendicularly to the fractures, while S waves result amplified in the same direction (see for instance Carcione et al. 2012, 2013). Such findings emphasize the importance of delineating the fault damage zones in the city planning and, as observed in the Etnean area where faults crosses villages, put into practice a specific strategy in order to takes into account these effects in the seismic code provisions.

## 5 Concluding remarks

A preliminary and quick seismic site response surveys, using ambient vibration measurements, was performed in the complex geologic setting such as the eastern flank of Mt. Etna. The obtained results can briefly be summarized as follow:

- The cluster analysis, based on the *k-means* technique, turned out to be a quite reliable procedure to subdivide HVNRs into four homogeneous classes of fundamental frequency.

- The results point out that lava flows, usually considered as stiff rock, are characterized by the presence of extensive areas where significant amplification effects take place. This behavior can be ascribed to the presence of alternating stiff and soft layers that very often characterize the lava successions. The complexity and heterogeneity characterizing the investigated area therefore imply that HVNR findings cannot be easily interpreted in term of the outcropping lithologies.
- Spectral ratio results also point out the outstanding heterogeneity of lava sequences making difficult to identify a single seismic bedrock formation.
- The contour map obtained by interpolating the frequency classes assigned to each measurement highlights the important role played by the fractures fields linked to the main fault systems.
- The analysis of directional seismic site effects and results from polarization diagrams of the horizontal components of motion allowed us to identify two main areas with strong directional effects striking NW–SE and WNW–ESE that appear almost perpendicular to the trend of PFS and TFS, respectively.

The used methodologies represent in our opinion the preliminary steps for a quick, practical, and inexpensive procedure to identify relevant macro-areas for future detailed studies aiming at reducing seismic risk in a very exposed region.

**Acknowledgments** The present study was performed in the frame of the Volcanologic Project DPC-INGV 2013–2015 “Multi-disciplinary analysis of the relationships between tectonic structures and volcanic activity” financially supported by the Italian Civil Protection Department (DPC). This paper does not necessarily represent the official opinion of the DPC.

## References

- Akaike H (1974) A new look at the statistical model identification. *IEEE Trans Autom Control* 19:716–723
- Azzaro R (2004) Seismicity and active tectonics in the Etna region: constraints for a seismotectonic model. In: Bonaccorso A, Calvari S, Coltelli M, Del Negro C, Falsaperla S (eds) *Mt. Etna: Volcano Laboratory*, vol 143. AGU Geophysical Monograph, Washington DC, pp 205–220
- Azzaro R, Barbano MS, Moroni AM, Mucciarelli M, Stucchi M (1999) The seismic history of Catania. *J Seismol* 3:235–252
- Azzaro R, Barbano MS, D’Amico S, Tuvè T, Albarello D, D’Amico V (2008) First study of probabilistic seismic hazard assessment in the volcanic region of Mt. Etna (southern Italy) by means of macroseismic intensities. *Boll Geof Teor Appl* 49(1):77–91
- Azzaro R, Carocci CF, Maugeri M, Torrisi A (2010) *Microzonazione sismica del versante orientale dell’Etna. Studi di primo livello. Regione Siciliana, Dipartimento della Protezione Civile, Le Nove Muse Editrice, Catania*, ISBN 978-88-87820-45-4. [http://sit.protezionecivilesicilia.it/index.php?option=com\\_content&view=article&id=24&Itemid=133](http://sit.protezionecivilesicilia.it/index.php?option=com_content&view=article&id=24&Itemid=133)
- Azzaro R, Branca S, Gwinner K, Coltelli M (2012) The volcano-tectonic map of Etna volcano, 1:100.000 scale: an integrated approach based on a morphotectonic analysis from high-resolution DEM constrained by geologic, active faulting and seismotectonic data. *Ital J Geosci* 131:153–170. doi:10.3301/IJG.2011.29
- Azzaro R, Bonforte A, Branca S, Gugliemino F (2013a) Geometry and kinematics of the fault systems controlling the unstable flank of Etna volcano (Sicily). *J Volcanol Geotherm Res* 251:5–15. doi:10.1016/j.jvolgeores.2012.10.001
- Azzaro R, D’Amico S, Peruzza L, Tuvè T (2013b) Probabilistic seismic hazard at Mt. Etna (Italy): the contribution of local fault activity in mid-term assessment. *J Volcanol Geotherm Res* 251:158–169
- Azzaro R, D’Amico S, Tuvè T (2016) Seismic hazard assessment in the volcanic region of Mt. Etna (Italy): a probabilistic approach based on macroseismic data applied to volcano-tectonic seismicity. *Bull Earthq Eng* 14:1813–1825
- Barreca G, Bonforte A, Neri M (2013) A pilot GIS database of active faults of Mt. Etna (Sicily): a tool for integrated hazard evaluation. *J Volcanol Geotherm Res* 251(1):170–186. doi:10.1016/j.jvolgeores.2012.08.013

- Bonforte A, Guglielmino F, Coltelli M, Ferretti A, Puglisi G (2011) Structural assessment of Mount Etna volcano from permanent scatterers analysis. *Geochem Geophys Geosyst* 12:Q02002. doi:[10.1029/2010GC003213](https://doi.org/10.1029/2010GC003213)
- Bonforte A, Federico C, Giammanco S, Guglielmino F, Liuzzo M, Neri M (2013) Soil gases and SAR data reveal hidden faults on the sliding flank of Mt. Etna (Italy). *J Volcan Geotherm Res* 251:27–40. doi:[10.1016/j.volgeores.2012.08.010](https://doi.org/10.1016/j.volgeores.2012.08.010)
- Branca S (2003) Geological and geomorphologic evolution of the Etna volcano NE flank and relationships between lava flow invasions and erosional processes in the Alcantara Valley (Italy). *Geomorphology* 53:247–261
- Branca S, Ferrara V (2001) An example of river pattern evolution produced during the lateral growth of a central polygenic volcano: the case of the Alcantara river system, Mt Etna (Italy). *Catena* 45(2):85–102
- Branca S, Ferrara V (2013) The morphostructural setting of Mount Etna sedimentary basement (Italy): implications for the geometry and volume of the volcano and its flank instability. *Tectonophysics* 586:46–64
- Branca S, Coltelli M, Groppelli G (2011a) Geological evolution of a complex basaltic stratovolcano: Mount Etna, Italy. *Ital J Geosci* 130(3):306–317. doi:[10.3301/IJG.2011.13](https://doi.org/10.3301/IJG.2011.13)
- Branca S, Coltelli M, Groppelli G, Lentini F (2011b) Geological map of Etna volcano, 1:50,000 scale Italy. *Ital J Geosci* 130(3):265–291. doi:[10.3301/IJG.2011.15](https://doi.org/10.3301/IJG.2011.15)
- Burnham KP, Anderson DR (2002) Model selection and multimodel inference: a practical information-theoretic approach, 2nd edn. Springer, New York
- Cara F, Cultrera G, Azzara RM, De Rubeis V, Di Giulio G, Giammarinaro MS, Tosi P, Vallone P, Rovelli A (2008) Microtremor measurements in the city of Palermo, Italy: analysis of the correlation with local geology and damage. *Bull Seism Soc Am* 98:1354–1372
- Carcione JM, Picotti S, Santos JE (2012) Numerical experiments of fracture-induced velocity and attenuation anisotropy. *Geophys J Int* 191:1179–1191. doi:[10.1111/j.1365-246X.2012.05697.x](https://doi.org/10.1111/j.1365-246X.2012.05697.x)
- Carcione JM, Gurevich B, Santos JE, Picotti S (2013) Angular and frequency dependent wave velocity and attenuation in fractured porous media. *Pure appl Geophys* 170(11):1673–1683. doi:[10.1007/s00024-012-0636-8](https://doi.org/10.1007/s00024-012-0636-8)
- D'Amico S, Meroni F, Sousa ML, Zonno G (2016) Building vulnerability and seismic risk analysis in the urban area of Mt. Etna volcano (Italy). *Bull Earthq Eng* 14:2031–2045
- Di Giulio G, Cara F, Rovelli A, Lombardo G, Rigano R (2009) Evidences for strong directional resonances in intensely deformed zones of the Pernicana fault, Mount Etna, Italy. *J Geophys Res* 114:B10308. doi:[10.1029/2009JB006393](https://doi.org/10.1029/2009JB006393)
- Eurocode8 (2003) Design of structures for earthquake resistance. Part1: general rules, seismic actions and rules for buildings. CEN European Committee for standardization, Brussels
- Finetti IR, Lentini F, Carbone S, Del Ben A, Di Stefano A, Forlin E, Guarnieri P, Pipan Y, Prizzon A (2005) Geological outline of Sicily and lithospheric tectono-dynamics of its Tyrrhenian margin from new CROP seismic data. In: Finetti IR (ed) CROP, Deep Seismic Exploration of the Mediterranean region, vol 15. Elsevier, Amsterdam, pp 319–376
- Gross F, Krastel S, Geersen J, Behrmann JH, Ridente D, Chiocci FL, Bialas J, Papenberg C, Cukur D, Urlaub M, Micallef A (2016) The limits of seaward spreading and slope instability at the continental margin offshore Mt Etna, imaged by high-resolution 2D seismic data. *Tectonophysics* 667:63–76
- Grünthal G (1998) European Macroseismic Scale 1998 (EMS-98). European Seismological Commission, subcommission on engineering seismology, working Group Macroseismic Scales. Conseil de l'Europe, Cahiers du Centre Européen de Géodynamique et de Séismologie, 15, Luxembourg, pp. 99, <http://www.ecgs.lu/cahiers-bleus/>
- Imposa S, De Guidi G, Grassi S, Scudero S, Barreca G, Patti G, Boso D (2015) Applying geophysical techniques to investigate a segment of a creeping fault in the urban area of San Gregorio di Catania, southern flank of Mt. Etna (Sicily–Italy). *J Appl Geophys* 123:153–163. doi:[10.1016/j.jappgeo.2015.10.008](https://doi.org/10.1016/j.jappgeo.2015.10.008)
- Jurkevics A (1988) Polarization analysis of three component array data. *Bull Seism Soc Am* 78:1725–1743
- Konno K, Ohmachi T (1998) Ground-motion characteristics estimated from spectral ratio between horizontal and vertical components of microtremor. *Bull Seism Soc Am* 88:228–241
- Langer H, Catalano S, Cristaldi M, De Guidi G, Gresta S, Monaco C, Tortorici L (1999) Strong ground motion simulation in the urban area of Catania on the basis of a detailed geological survey. In: Orvieto G, Brebbia CA (eds) Earthquake resistant engineering structures. WIT Press Southampton, Boston, pp 343–352
- Lavecchia G, Ferrarini F, de Nardis R, Visini F, Barbano MS (2007) Active thrusting as a possible seismogenic source in Sicily (southern Italy): some insights from integrated structural-kinematic and seismological data. *Tectonophysics* 445:145–167

- Lentini F, Carbone S, Guarnieri P (2006) Collisional and postcollisional tectonics of the Apenninic-Maghrebien orogen (southern Italy). In: Dilek Y, Pavlides S (eds) Postcollisional tectonics and magmatism in the Mediterranean region and Asia. GSA Special Paper 409, pp 57–81
- Lermo J, Chavez-Garcia FJ (1993) Site effect evaluation using spectral ratios with only one station. *Bull Seism Soc Am* 83(5):1574–1594
- MacQueen JB (1967) Some methods for classification and analysis of multivariate observations. In: Proceedings of 5th Berkeley symposium on mathematical statistics and probability, vol 1. University of California Press, Berkeley, pp 281–297
- Maresca R, Castellano M, De Matteis R, Saccorotti G, Vaccariello P (2003) Local site effects in the town of Benevento (Italy) from noise measurements. *Pure appl Geophys* 160:1745–1764
- Mucciarelli M (1998) Reliability and applicability of Nakamura's technique using microtremors: an experimental approach. *J Earthq Eng* 2:625–638
- Nakamura Y (1989) A method for dynamic characteristics estimation of subsurface using microtremor on the ground surface. *Quart Rep Railw Tech Res Inst* 30:25–33
- Neri M, Acocella V, Behncke B (2004) The role of the Pernicana fault system in the spreading of Mt. Etna (Italy) during the 2002–2003 eruption. *Bull Volcanol* 66:417–430. doi:10.1007/s00445-003-0322-x
- Neri M, Casu F, Acocella V, Solaro G, Pepe S, Berardino P, Sansosti E, Caltabiano T, Lundgren P, Lanari R (2009) Deformation and eruptions at Mt. Etna (Italy): a lesson from 15 years of observations. *Geophys Res Lett* 36(2):L02309. doi:10.1029/2008GL036151
- Nogoshi M, Igarashi T (1971) On the amplitude characteristic of microtremor (part 2) (in Japanese with English abstract). *J Seismol Soc Jpn* 24:26–40
- Panzerà F, Lombardo G, Rigano R (2011a) Use of different approaches to estimate seismic hazard: the study cases of Catania and Siracusa, Italy. *Boll Geofis Teor Appl* 52(4):687–706. doi:10.4430/bgta0027
- Panzerà F, Rigano R, Lombardo G, Cara F, Di Giulio G, Rovelli A (2011b) The role of alternating outcrops of sediments and basaltic lavas on seismic urban scenario: the study case of Catania, Italy. *Bull Earthq Eng* 9(2):411–439. doi:10.1007/s10518-010-9202-x
- Panzerà F, Lombardo G, Muzzetta I (2013) Evaluation of buildings dynamical properties through in-situ experimental techniques and 1D modelling: the example of Catania, Italy. *Phys Chem Earth* 63:136–146. doi:10.1016/j.pce.2013.04.008
- Panzerà F, Pischiutta M, Lombardo G, Monaco C, Rovelli A (2014) Wavefield polarization in fault zones of the western flank of Mt. Etna: observations and fracture orientation modelling. *Pure appl Geophys* 171(11):3083–3097. doi:10.1007/s00024-014-0831-x
- Panzerà F, Lombardo G, Monaco C, Di Stefano A (2015) Seismic site effects observed on sediments and basaltic lavas outcropping in a test site of Catania, Italy. *Nat Hazards* 79(1):1–27. doi:10.1007/s11069-015-1822-7
- Panzerà F, Lombardo G, Monaco C (2016) New evidence of wavefield polarization on fault zone in the lower NE slope of Mt. Etna. *Ital J Geosci* 135(2):250–260. doi:10.3301/IJG.2015.22
- Pischiutta M, Rovelli A, Salvini F, Di Giulio G, Benzon Y (2013) Directional resonance variations across the pernicana fault, Mt. Etna, in relation to brittle deformation fields. *Geophys J Int* 193(2):986–996. doi:10.1093/gji/ggt031
- Pischiutta M, Pastori M, Improta L, Salvini F, Rovelli A (2014) Orthogonal relation between wavefield polarization and fast S-wave direction in the Val d'Agri region: an integrating method to investigate rock anisotropy. *J Geophys Res* 119:1–13. doi:10.1002/2013JB010077
- Polonia A, Torelli L, Artoni A, Carlini M, Faccenna C, Ferranti L, Gasperini L, Govers R, Klaeschen D, Monaco C, Neri G, Nijholt N, Orecchio B, Wortel R (2016) The Ionian and Alfeo–Etna fault zones: new segments of an evolving plate boundary in the central Mediterranean Sea? *Tectonophysics* 675:69–90
- Rigano R, Cara F, Lombardo G, Rovelli A (2008) Evidence for ground motion polarization on fault zones of Mount Etna volcano. *J Geophys Res* 113:B10306. doi:10.1029/2007JB005574
- Rodriguez VH, Midorikawa S (2002) Applicability of the H/V spectral ratio of microtremors in assessing site effects on seismic motion. *Earthq Eng Struct Dyn* 31(2):261–279
- Romanelli F, Vaccari F (1999) Site response estimation and ground motion spectrum scenario in the Catania area. *J Seismol* 3:311–326
- SESAME (2004) Guidelines for the implementation of the H/V spectral ratio technique on ambient vibrations: measurements, processing and interpretation. SESAME European Research Project WP12, deliverable D23.12, at <http://sesame-fp5.obs.ujfgrenoble>